



Late Permian paleoclimatic record in the southwest Gondwana Supercontinent: evidence from clay minerals and gamma-ray spectrometry in Paraná Basin, State of Santa Catarina, southern Brazil

Costa, H.S., LPGA-UFPR; Nascimento, M.S., ANBA-UFSC; Ferreira, F.J.F., LPGA-UFPR

Copyright 2018, SBGf - Sociedade Brasileira de Geofísica

Este texto foi preparado para a apresentação no VIII Simpósio Brasileiro de Geofísica, Salinópolis, 18 a 20 de setembro de 2018. Seu conteúdo foi revisado pelo Comitê Técnico do VIII SimBGf, mas não necessariamente representa a opinião da SBGf ou de seus associados. É proibida a reprodução total ou parcial deste material para propósitos comerciais sem prévia autorização da SBGf.

Abstract

The Rio do Sul and Rio Bonito formations in the region of Rancho Queimado in the state of Santa Catarina, southern Brazil, record environmental changes related to climate fluctuations during the drift of the supercontinent Gondwana from the south pole to the Earth's equatorial region. These paleoclimatic variations were have been assessed by clay mineral analysis and gamma-ray spectrometric patterns of outcrops. The data obtained indicate that detrital illite content makes up approximately 50 to 60 % of the clay mineral assemblage. The low eTh/K and eTh/eU ratios and the detrital illite in the strata of the Rio Bonito Formation indicate a cold and dry climate during deposition. The contrast between the increase in eTh/K and eTh/eU ratios and the decrease in the illite content toward the top of the Rio Bonito Formation suggests progressively warmer and humid climatic conditions.

Introduction

The sedimentary stratigraphic record suggests that glaciations have occurred episodically throughout the earth's history (Crowell, 1999). One of those glaciations affected the Gondwana Supercontinent during the late Paleozoic and constituted the longest period of continuous glaciation in the Phanerozoic (Eyles, 2003). Carboniferous to Early Permian glaciogenic sedimentary rocks have been identified on all subcontinents of Gondwana, such as, South America (Buatois & Mangano, 1995; López-Gamundí, 1997; Archanjo et al., 2006), Africa (Scheffler et al., 2003), India (Maejima et al., 2004), Australia (Scheffler et al., 2003), and Antarctica (Collinson et al., 1994; Isbell et al., 2003). This glacial age is subdivided into three episodes (López-Gamundí, 1997): glacial episode I (Late Devonian-Earliest Carboniferous), glacial episode II (Late Carboniferous), and glacial episode III (Late Carboniferous-Early Permian). Sedimentological and stratigraphic studies of Permo-Carboniferous sedimentary rocks in the Paraná Basin have suggested a transition of the glacial period to the subsequent global warming that controlled the deep paleoenvironmental change caused by transgression-regression of the Panthalassa at the western edge of the Gondwana Supercontinent (Fig. 1A and 1B). Climate change during late deposition of the Rio do Sul Formation

(Itararé Group) and early deposition of the Rio Bonito Formation (Guatá Group) has been insufficiently studied. Most of the studies on climate records in the Itararé and Guatá Groups (Fig. 1A, 1B and 1C) were based on paleoenvironmental and stratigraphic data (Goldberg, 2001; Holz & Kalkreuth, 2002; Slonsk, 2002; Cancela, 2008). This work presents gamma-ray spectrometric patterns of eTh/K, eTh/U ratios and clay minerals to investigate the paleoclimatic signature during the late sedimentation of the Taciba/Rio do Sul Formation and the early sedimentation of the Rio Bonito Formation in the eastern portion of the Paraná Basin (Fig. 1C). Gamma-ray spectrometric data reveal important information on paleoclimatic changes (Ruffell and Worden, 2000), and petrographic data may reveal sedimentary provenance in different tectonic environments (Dickinson, 1985).

Methods

The stratigraphic sections of the Rio do Sul and Rio Bonito Formations were examined and logged at four localities of the Rancho Queimado region (Fig. 1A). The exposures were at road cuttings along the BR-282 (Fig. 1A). The study outcrops have a wide lateral (> 30 m) and vertical (5 to 15 m) exposure and include the uppermost portion of the Rio do Sul Formation (BP.09 and BP.67) and the lowermost portion of the Rio Bonito Formation (BP.72 and BP.73) in this region. Four stratigraphic sections on the studied outcrops (BP.67, BP.09, BP.72 and BP.73, Fig. 1) were made. Twelve sandstone thin sections from the Rio do Sul Formation and seven thin sections from the Rio Bonito Formation were analyzed under an optical microscope at the Sedimentary Basin Laboratory (LABAC/UFSC). The diagenetic constituents and clay minerals were studied using a Scanning Electron Microscope (SEM) (JEOL JSM 6010LA) at both the Central Laboratory of Scanning Electron Microscopy (LCME/UFSC), and Laboratory of Minerals and Rocks (LAMIR/UFPR). Four samples of shales were taken from each formation to analyze clay mineral associations using X-ray diffraction (XRD) on a PANalytical model X PertPRO-MPD (LAMIR/UFPR) equipped with a vertical goniometer of 240 mm and a linear detector with a 2,122° opening (Xcelerator). The spectral radiometric signatures were obtained using the RS-230 handheld gamma-ray spectrometer (Radiation Solutions, Canada) from the Laboratory for Research in Applied Geophysics (LPGA/UFPR). The equipment has a detector with a bismuth germanium oxide (BGO) crystal with 6.3 in³ (103 cm³) sensitivity. The readings were obtained in counts per minute (cpm) for each element and total count (TC) in parts per million (ppm) for uranium (eU), % for potassium (K) and ppm for uranium (eU) and thorium (eTh). The

data were acquired with spacing of 10 cm (sensor diameter) and an integration time of 120 s. The readings were performed with the instrument positioned perpendicularly to the strata surface. The measured data were stored in the apparatus and transferred to a computer for analysis using RS-Analyst software.

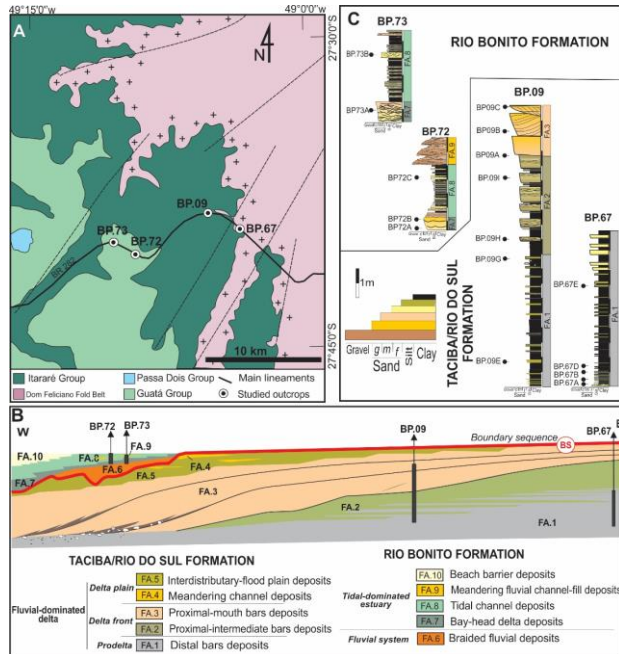


Figure 1 - (A) Geological map of the study area in Rancho Queimado region, with location of outcrops; (B) Schematic stratigraphic section demonstrating the relationship between the main facies and related paleoenvironments; (C) Logged sections of the outcrops with the position of the analyzed samples.

Results

The clay minerals in the Rio do Sul and Rio Bonito Formations include illite, vermiculite, and interlayered illite-smectite and chlorite (Figs. 2 and 3). The illite was identified by reflections at 10 Å and the vermiculite by reflections at 4.3 Å. Octahedral smectite and quartz traces occur. The illite occurs in all samples of the Rio do Sul Member and was not identified in the Rio Bonito Formation (Fig. 3). The illite-smectite interlayers generally occur with associated illite crystals. Illite is the main clay mineral in the Rio do Sul Formation, constituting 50 % to 60 % of the assemblage, and SEM micrographs show dioctahedral-trioctahedral illite (Fig. 2). Vermiculite constitutes 20 % of the clay mineral assemblage in the middle to upper portions of the Rio do Sul Formation. Illite-smectite interlayers represent approximately 1 % of the assemblage. Chlorite was found in only the Rio Bonito Formation (Fig. 3, BP.73).

Gamma-ray spectrometry is a valuable technique to combine with fieldwork to recognize the effect of climatic control on sedimentation. The TC, K, eU and eTh patterns

in the Rio do Sul Formation were interpreted in two profiles, as shown in Figure 4.

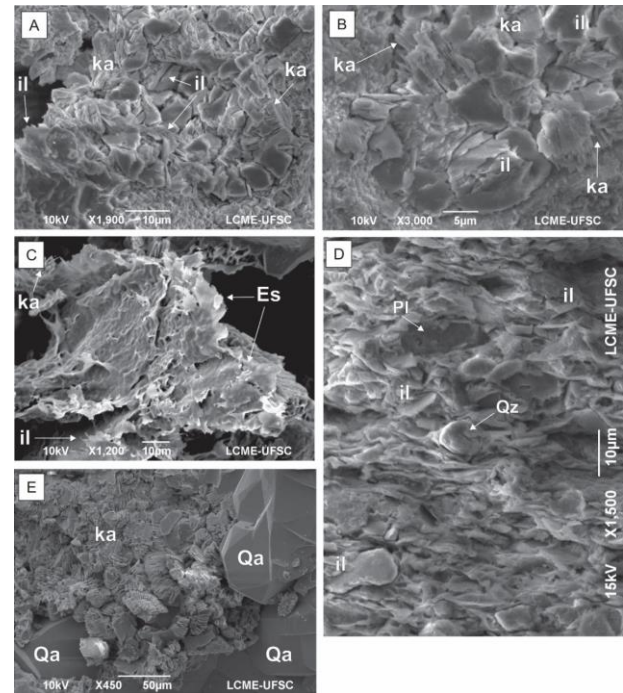


Figure 2 - SEM micrograph of the Rio do Sul and Rio Bonito Formations: (A-B) illite (il), quartz grains (Qz) and booklet kaolinite (ka) in sandstones; (C) smectite (Sm) and illite; (D) illite parallel to the lamination, contouring the silty-quartz (Qz) and plagioclase (Pl); and (E) booklet kaolinite and authigenic quartz (Qa).

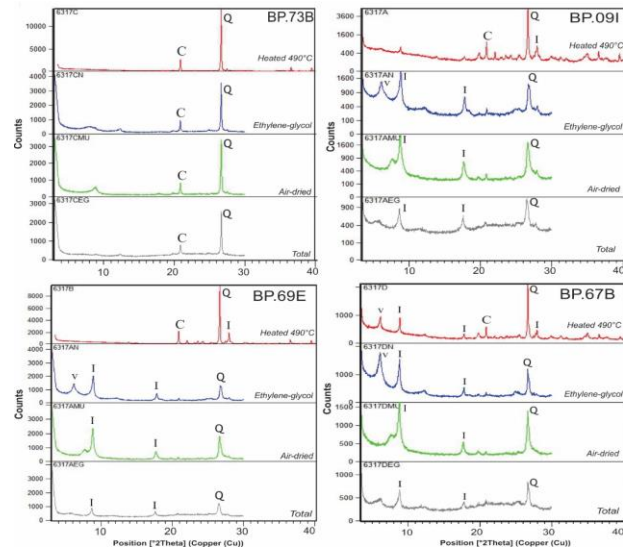


Figure 3 - XRD traces of main clay minerals (air-dry, ethylene glycol-solvated and heated to 450°C) of the Rio do Sul and Rio Bonito Formations. Illite (I), vermiculite (v), quartz (Q) and chlorite (C).

Spectral gamma-ray logs of the sandstones have lower K concentrations (Fig. 4, BP.09 top), ranging from 1.2 to 2.4 %. In contrast, eU presents values approximately 17.9 ppm, having a minimum value of 7.1 ppm, and eTh presents the highest value in this lithofacies (31.0 to 45.9 ppm). The eU and eTh have values of 14 and 40 ppm, respectively. In these two lithofacies, TC values show direct correlation with eU and eTh concentrations. The shales show the values range between 2.1 % and 4.9 % (Tab. 1). The eU and eTh show values between 3.6 and 14.3 ppm and between 19.2 and 48.3 ppm, respectively. In general, this result indicates that the concentrations of these radionuclides present a gradual increase from the base (Fig. 4, BP.09) to the top (Fig. 4, BP.67) of the session. The TC curves are similar to the curves of K, eU and eTh, showing the relationship with these three elements. The character of the gamma-ray log through the investigated sections shows an upward increase in the concentrations of these radionuclides, illustrating consistency with TC data. However, there is no significant variation in the eTh/K and eTh/eU ratios since growth is equivalent to the K, eU and eTh concentrations. The eTh/K and eTh/eU ratios from bottom to top of the session show low and relatively homogeneous values (7 for eTh/K, 2 and 8 for eTh/eU). Two gamma-ray profiles were measured in the Rio Bonito Formation (Fig. 5), and data from each lithofacies, including TC, K, eU and eTh concentrations, are listed in Table 1. In the sandstones at the base and top portions of this stratigraphic unit (Fig. 5, BP.73 and BP.72), the K values range from 1.2 to 2.6 %, and the eU signatures have values from 2.3 to 28.6 ppm. The sandstones at the base of the BP.73 profile (Fig. 5) produce eTh values that gradually increase toward the top of the section. In contrast, the sandstones at the base of the log from BP:72 (Fig. 5), show values ranging from 12 to 17 ppm from the bottom to the top. The TC data are similar to curves of eU and eTh, indicating the influence of these radionuclides on the TC values. The pelites of the Rio Bonito Formation exhibit K contents from 1.8 to 4.2 % (in the lower portion of the BP.73 profile, Fig. 5,) and from 2.6 to 3.2 % (in the upper portion of the BP.72 profile, Fig. 5). The eU measurements are similar to the K measurements, with 14.7 ppm at the base to 3.0 ppm in the upper portion of the section. At the base of the secession, the eTh values range from 14.2 to 23.5 ppm and strongly correlate with eTh from the upper portion. The TC data have similar patterns to K, eU and eTh, indicating the influence of these radionuclide concentrations. The gamma-ray data of the Rio Bonito Formation show a significant upward decrease in the radionuclides concentration, which is more evident in to TC data. The variations in the eTh/K and eTh/eU ratios are not expressive (~ 5), but with peaks at ~ 7 . The increase in eTh/K ratios is noted mainly in the sandstones (14 to 25 ppm), but not accompanied by the eTh/eU ratios, which show a small decrease (~ 2) in relation to the general pattern (~ 2.5 to 7). The low eTh/eU ratio results from the relative increase in eU concentration in this sedimentary facies.

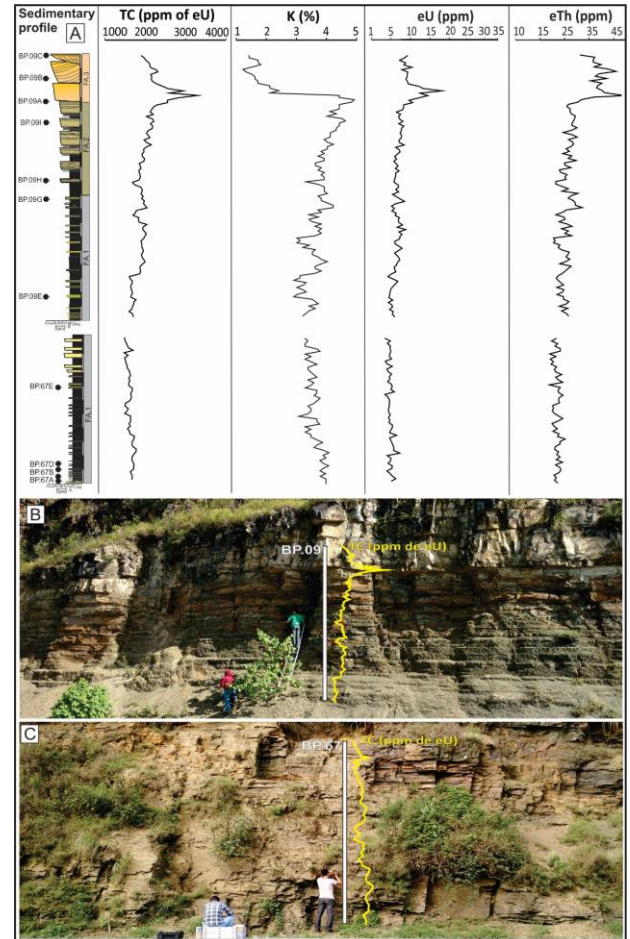


Figure 4 - (A) Sedimentary logs with facies associations, including sample locations and gamma-ray signatures (TC, K, eU and eTh); and (B and C) Field photographs of the outcrops in the Rio do Sul Formation (BP:09 and BP:67, respectively).

Discussion

The clay mineral assemblage is a significant indicator of paleoclimatic regimes, paleotectonic processes and diagenetic processes. Detrital or authigenic clay minerals are widely used to determine the climatic conditions during sediment deposition (Parry & Reeves 1968; Singer 1984; Chamley 1989; Tucker 2001; Gonçalves et al., 2006). Illite is the main clay mineral in the Rio do Sul Formation and is ca. 50 to 60 % of the assemblage, especially in the rhythmites and fine-grained sandstones. According to Velde (1995), the illite formation includes slow weathering processes, even in an environment with high-K availability. The lack of occurrence of smectite in these formations suggests a detrital origin of the illite. The rich Na⁺-K⁺ environments aid in the formation of mixed layers and micas. Vermiculite has a structure similar to smectite, although it is less expandable (Tucker, 2001), indicating leaching of K-feldspar (Kf) during diagenesis or weathering of muscovite under good drainage and low-pH conditions that are very abundant in both fine-grained sandstone and rhythmites.

Acknowledgments

The authors thank to Petrobras for supporting this research under the contract PFRH240-PB-UFSC. We are very grateful to Almério Barros França, Leonardo Fadel Cury and Valter Antonio Becegato for their suggestions and assistance in the LAMIR/UFPR laboratory, and to Itaipu Binacional by the lending of the gamma-ray spectrometer. F.J.F. Ferreira thanks the support of the National Council for Scientific and Technological Development (CNPq) for this study, under contract 306978/2015-6.

References

- Buatois, L.A., Mangano, M.G., 1995. The paleoenvironmental and paleoecological significance of the lacustrine *Mermia* ichnofacies: An archetypical subaqueous nonmarine trace fossil assemblage. *Ichnos* 4, 151–161.
- Cacela, A.S.M., 2008. Paleoclima e dinâmica costeira como fatores controladores da distribuição de arenitos em sistemas paralíticos – Um estudo para reservatórios análogos no Eopermiano da Bacia do Paraná. Dissertação de Mestrado, Instituto de Geociências, Universidade Federal do Rio Grande do Sul, Brasil.
- Chamley, H., 1989. *Clay Sedimentology*. Springer-Verlag, Berlin, 623.
- Crowell, J. C., 1999. Pre-Mesozoic ice ages: Their bearing on understanding the climate system. *Geological Society of America Memoir* 192.
- Dickinson, W.R., 1985. Interpreting provenance relations from detrital modes of sandstones. In: Zuffa, G.G. (Eds.), *Provenance of Arenites*. Reidel Publ., Dordrecht, 333 – 361.
- Eyles, C.H., Mory, A.J., Eyles, N., 2003. Carboniferous-Permian facies and tectono-stratigraphic successions of the glacially influenced and rifted Carnarvon Basin, western Australia. *Sedimentary Geology* 155, 63–86.
- Gonçalves, D.F.; Rossetti, D.F.; Truckenbrodt, W.; Mendes, A. C., 2006. Argilominerais da Formação Codó (Aptiano Superior), Bacia de Grajaú, Nordeste do Brasil. *Latin American Journal of Sedimentology and Basin Analysis* 13, 59-75.
- Goldberg, K., 2001. *The Paleoclimatic Evolution of the Permian of the Paraná Basin in southern Brazil*. Ph.D. Dissertation, Department of Geophysical Sciences, University of Chicago, 267 pp.
- Holz, M., Kalkreuth, W., 2002. Sequence Stratigraphy and Coal Petrology applied to the Early Permian coal-bearing Rio Bonito Formation, Paraná Basin, Brazil. *American Association of Petroleum Geology, Special Publication*, 45-56.
- López-Gamundí, O.R., 1997. Glacial-postglacial transition in the late Paleozoic basins of southern South America, in Martini, I.P., (Eds.), *Late Glacial and Postglacial Environmental Changes*. Oxford, UK, Oxford University Press, 147-168.
- Maejima, W., Das, R., Pandya, K.L., Hayashi, M., 2004. Deglacial control on sedimentation and basin evolution of Permo-Carboniferous Talchir Formation, Talchir Gondwana Basin, Orissa, India. *Gondwana Research* 7, 339-352.
- Menezes, M.T.F., Nascimento, M.S., 2015. Petrografia e diagênese de arenitos permianos da Bacia do Paraná, região de Alfredo Wagner, Santa Catarina IX SIMPÓSIO SULBRASILEIRO DE GEOLOGIA. Florianópolis, Santa Catarina. Sociedade Brasileira de Geologia Núcleo RS/SC. Boletim de resumos, p.15.
- Milani E.J., Melo J.H.G., Souza P.A., Fernandes L.A., França A.B., 2007. Bacia do Paraná. In: Milani E.J., Rangel H.D., Bueno G.V., Stica J.M., Winter W.R., Caixeta J.M., Pessoa Neto O.C., (Eds.), *Bacias Sedimentares Brasileiras - Cartas Estratigráficas*. Boletim de Geociências da Petrobras, Rio de Janeiro, 15(2): 265-287.
- Parry, W.T., C.C., Reeves, 1968. Clay mineralogy of pluvial lake sediments, Southern High Plain, Texas. *Journal of Sedimentary Petrology* 38, 516-529.
- Ruffell, A., Worden, R., 2000. Palaeoclimate analysis using spectral gamma-ray data from the Aptian (Cretaceous) of southern England and southern France. *Palaeogeogr. Palaeoclimatol.*, 155(3-4), 265-283.
- Scheffler, K., Hoernes, S., Schwark, L., 2003. Global changes during Carboniferous–Permian glaciation of Gondwana: Linking polar and equatorial climate evolution by geochemical proxies. *Geology*, 31(7), 605-608.
- Schnyder, J., Ruffell, A., Deconinck, J.F., Baudin, F., 2006. Cojuntive use of spectral gamma – ray logs and clay minerals in drilling Late Jurassic to Early Cretaceous paleoclimate change (Dorset, U.K.). *Paleo. Paleo. Paleo.* 229, 303-320.
- Singer, A., 1984. The paleoclimatic interpretation of clay minerals in sediments-a review. *Earth Science Reviews* 21, 251-293.
- Slonski, G.T., 2002. *Interpretação paleoclimática do Permiano Inferior da Bacia do Paraná em Santa Catarina, Brasil (Formação Rio Bonito)*. Dissertação de Mestrado, Centro de Ciências Biológicas, Universidade Federal de Santa Catarina, Brasil.
- Tucker, M.E., 2001. *Sedimentary Petrology: an introduction to the origin of sedimentary rocks*. 3rd edition, Oxford, Blackwell, 262 pp.
- Velde, B., 1995. *Origin and mineralogy of clay minerals*. Springer, Berlin. 334p.

Table 1. Gamma-ray spectrometric data from sandstones and shales of the Rio do Sul and Rio Bonito Formation.

Rio do Sul Formation	Sandstones (16 samples)				Shales (153 samples)			
Elements	TC (ppm/eU)	K (%)	eU (ppm)	eTh (ppm)	TC (ppm/eU)	K (%)	eU (ppm)	eTh (ppm)
Mean	2240.82	1.60	9.77	38.65	1855.87	3.70	6.02	24.80
Standard deviation	248.82	0.30	2.62	3.32	249.53	0.40	1.55	3.75
Variation coefficient	0.11	1.18	0.26	0.08	0.13	0.10	0.25	0.15
Maximum	2945.20	2.40	17.90	45.90	3302.20	4.90	14.30	48.30
Minimum	1919.70	1.20	7.10	31.30	1532.50	2.10	3.60	19.20
Rio Bonito Formation	Sandstones (38 samples)				Shales (63 samples)			
Elements	TC (ppm/eU)	K (%)	eU (ppm)	eTh (ppm)	TC (ppm/eU)	K (%)	eU (ppm)	eTh (ppm)
Mean	1693.01	1.84	10.70	19.90	1677.07	3.06	7.70	19.50
Standard deviation	681.60	0.40	8.00	6.00	336.29	0.63	3.10	2.30
Variation coefficient	0.40	0.21	0.74	0.30	0.20	0.20	0.40	0.11
Maximum	3166.00	2.60	28.60	30.90	2177.30	4.20	14.70	23.50
Minimum	923.30	1.20	2.30	11.50	1140.00	1.80	3.00	14.20